Topology of spin polarization of the 5*d* states on W(110) and Al/W(110) surfaces

A. G. Rybkin,[1] E. E. Krasovskii,[2,3,4] D. Marchenko,[1,5] E. V. Chulkov,[2,4,6] A. Varykhalov,[5] O. Rader,[5] and A. M. Shikin[1]

[1]*Physical Department, St. Petersburg State University, 198504 St. Petersburg, Russia*
[2]*Department of Materials Physics, University of the Basque Country UPV/EHU, 20080 Donostia-San Sebastián, Spain*
[3]*IKERBASQUE, Basque Foundation for Science, 48011 Bilbao, Spain*
[4]*Donostia International Physics Center (DIPC), 20018 Donostia-San Sebastián, Spain*
[5]*Helmholtz-Zentrum Berlin für Materialien und Energie, Elektronenspeicherring BESSY II,*
Albert-Einstein-Straße 15, D-12489 Berlin, Germany
[6]*Centro de Física de Materiales CFM - Materials Physics Center MPC, Centro Mixto CSIC-UPV/EHU, Edificio Korta, Avenida de Tolosa 72,*
20018 San Sebastián, Spain

The spin polarization of W(110) and Al/W(110) surfaces is studied by spin- and angle-resolved photoemission. On both surfaces distinct $E(\mathbf{k}_\parallel)$ dispersions are identified with an unusual topology: A single spectral branch is spin polarized antisymmetrically relative to the $\bar{\Gamma}$ point, and two spin-polarized branches cross at $\bar{\Gamma}$. The crossing branches disperse linearly but this similarity to a Dirac cone is lost after deposition of the Al, where they acquire a parabolic dispersion. Based on *ab initio* one-step photoemission theory, we show that the measured spin polarization is a property of the ground state and identify the effect as the counterpart of the recently discovered Rashba polarization of bulk states at the surface, but with a distinct non-Rashba topology.

PACS number(s): 73.20.−r, 71.15.Ap, 71.70.Ej

I. INTRODUCTION

The importance of spin filter materials for spintronics has attracted great interest to the spin structure of crystal surfaces. In the absence of magnetic fields a spin polarization of the surface is caused by the spin-orbit interaction, which for strictly two-dimensional (2D) surface or interface states leads to their energy splitting and spin polarization. For a lattice with a 3D inversion symmetry this is the Rashba-Bychkov (RB) effect,[1] where the splitting is due to a potential gradient perpendicular to the surface. The situation becomes even more interesting in insulating solids: Depending on the symmetry of the bulk band structure, the conducting 2D gap states fall into two topologically distinct classes: trivial ones (e.g., the RB split states) and topological states protected by time-reversal symmetry (the case of a topological insulator, TI). In the two classical cases one can unambiguously indicate two spin-counterpart states for a given Bloch vector $\mathbf{k}_\parallel$ parallel to the surface. The difference is that in the RB case the dispersion lines $E(k_\parallel)^{\uparrow\downarrow}$ are crossed an even number of times by the Fermi level, whereas in the TI case the number is odd.[2–4] The natural question arises as to how metal surfaces of heavy elements, which provide the necessary strong spin-orbit interaction, behave in this respect. The RB effect was first measured on Au(111), Ref. 5, and a more complex so-called "topological metal" state was found on Bi(114), Ref. 6, and Sb(111), Ref. 7, which has been related to the topological surface states of topological insulators.[2,8]

The present paper addresses the spin spectral density of *d*-type electronic states. We study the clean W(110) surface and its modification by an Al monolayer with a combined experimental and theoretical spin- and angle-resolved photoelectron spectroscopy (SARPES). The 2D states brought about by thin films on W(110) are strongly influenced by the spin-orbit interaction in the substrate.[9–15] This was first established for Li/W(110) in Ref. 9, and the spin polarization of the overlayer states was first measured for H/W(110) in

Ref. 10. Overlayers of noble metals[11–13] and aluminum[14] also show large spin-orbit splitting caused by the substrate, since it is much smaller on Mo(110) than on W(110).[9,11]

The classical RB effect results in a shift of 2D states of opposite spin in opposite $\mathbf{k}_\parallel$ directions; see Fig. 1(a). It has recently been shown that surprisingly also in 3D continuum bands it leads to a $\mathbf{k}_\parallel$-dependent surface spin polarization.[16,17] Even though the Kramers degeneracy of the 3D states is not lifted, a polarization at the surface occurs due to a spin-dependent reflection of the Bloch waves from the surface. Here the net-spin $\mathbf{k}_\parallel$ projected density of states (DOS) $S(E,\mathbf{k}_\parallel)$ has an energy distributed character (unlike the δ function for the 2D states), which is large enough to cause a strongly spin-polarized photoemission detectable because the experiment is very surface sensitive. This effect was reported for the Bi(111) surface in Ref. 16. Here we show that the $S(E,\mathbf{k}_\parallel)$ function of W(110) and Al/W(110) surfaces exhibits distinct net-spin dispersion branches $E(\mathbf{k}_\parallel)$, which merge into the surface states in the $\mathbf{k}_\parallel$ projected bulk gaps and show a topology that is qualitatively different from the classical RB picture and reminiscent of topological surface states; see Fig. 1(b).

In the present work, we report on the experimental observation of strongly spin-polarized surface resonances and show that their dispersion changes from linear in a wide $k_\parallel$ range around $\bar{\Gamma}$ in W(110) to parabolic in Al/W(110). We analyze these results by *ab initio* calculations of the ground-state spin density distribution and by one-step calculations of the photocurrent. The photoemission process is found to influence the spin polarization of the photocurrent: In particular, it causes a polarization of normal-emission spectra. Nevertheless, the measured unusual spin topology is traced to the ground state, i.e., to the $S(E,\mathbf{k}_\parallel)$ function of W(110) and Al/W(110) surfaces, which exhibits distinct net-spin dispersion branches $E(\mathbf{k}_\parallel)$. In the $\mathbf{k}_\parallel$ projected bulk gaps they appear as surface states, and in the 3D bulk band they have

the same origin as recently reported Rashba-polarized bulk states,[16,17] but with a band topology different from the RB case.

II. EXPERIMENT

The experiments were carried out at the Russian-German UE112-PGM and U125/2-SGM beamlines at BESSY II with a "Phoibos" hemispherical analyzer and a Mott spin detector operating at 26 keV. Cleaning of the W(110) surface and the deposition of Al was carried out using standard methods.[11–15] The Al layer thickness was calibrated by the analysis of the Al derived quantum well state QWS1.[14,15] The spectra for two directions of spin (spin-↑ and spin-↓) perpendicular to the emission plane were measured with a *p* polarized light of $\hbar\omega = 62$ eV. The light incidence angle was fixed at 55° relative to the analyzer axis, and the off-normal emission in the direction $\bar{\Gamma}\bar{S}$ was measured by rotating the sample.

III. RESULTS AND DISCUSSION

The measured $\mathbf{k}_\parallel$ dispersion of the emission intensity along $\bar{\Gamma}\bar{S}$ is shown in Fig. 1(d) for the pure W(110) surface and
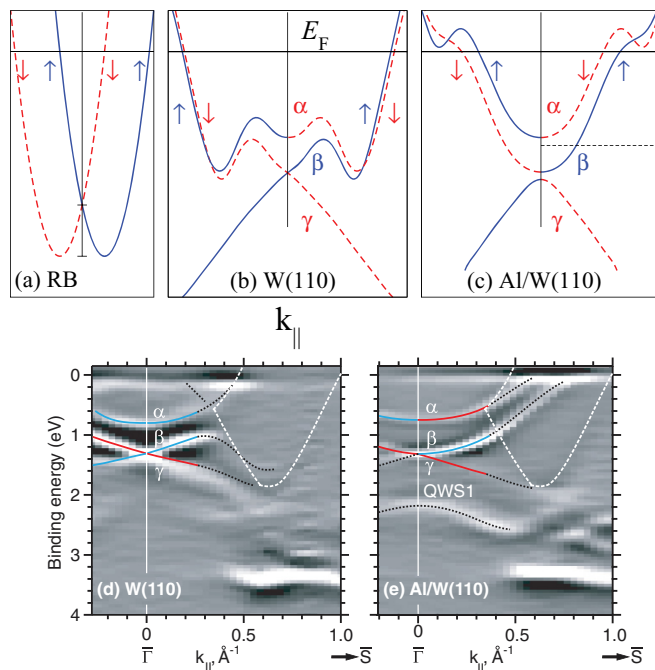

FIG. 1. (Color online) Topology of the spin branches for the RB case (a) and for the $\bar{\Gamma}\bar{S}$ direction of W(110) (b) and Al/W(110) (c): spin-↑ (blue solid lines) and spin-↓ (red dashed lines). The dashed horizontal line in graph (c) shows that over a finite energy interval between the bottom of α and bottom of β the constant-energy line is crossed only once by the branch β and is not crossed by its spin counterpart. SARPES measurements for clean W(110) (d) and for Al/W(110) (e) as the second derivative of the photocurrent. Black dashed lines show the dispersion of the ARPES intensity maxima in the regions where spin-resolved measurements are not available. The white dashed line marks the $\mathbf{k}_\parallel$ projected bulk band gap. QWS1 in graph (e) stands for the Al derived quantum-well state. The spatial localization of QWS1 is demonstrated in the calculated density map, Fig. 4(h). The spin assignment in graphs (d) and (e) is derived from the spectra presented in Fig. 2.
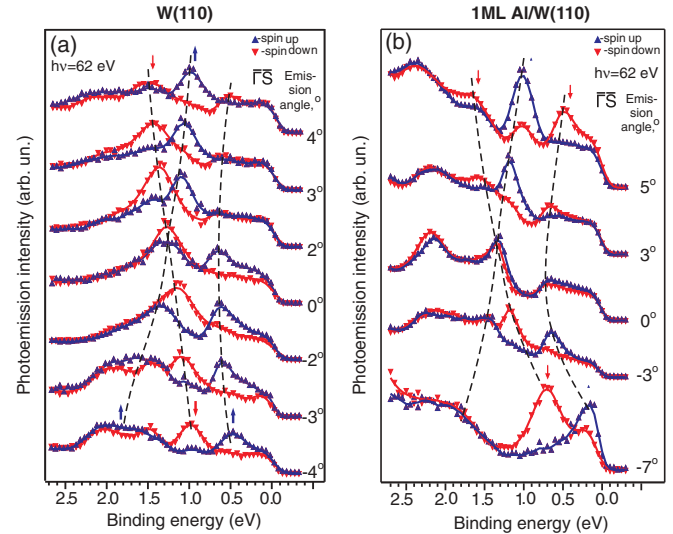

FIG. 2. (Color online) Spin- and angle-resolved energy distribution curves (EDCs) for clean W(110) (a) and for Al/W(110) (b). Photocurrent of spin-↓ is shown by blue upward triangles and spin-↑ by red downward triangles.

in Fig. 1(e) for the surface covered by 1 monolayer of Al. The assignment of spectral maxima to spin-↑ (blue lines) and spin-↓ (red) in Figs. 1(d) and 1(e) is derived from the SARPES spectra shown in Fig. 2. For W(110) the dispersions agree well with earlier measurements.[9,15,18–20] At normal emission, most pronounced is the surface resonance at 1.3 eV in the spin-orbit pseudogap[18] (between Γ_{7+} and Γ_{8+}; Ref. 21). It gives rise to the dispersion branches β and γ in Fig. 1(d), and the band edge at $E_{\bar{\Gamma}} = 0.8$ eV disperses as branch α. The measured spin-↓ branch γ disperses from 1.3 eV at $\bar{\Gamma}$ to 2.3 eV at $k_\parallel = 0.6$ Å^{-1}, where it merges with the edge of the $\bar{\Gamma}\bar{S}$ projected gap. The oppositely polarized branch β rises to reach the gap edge at 0.4 Å^{-1}. The branch β retains its surface-resonance character well away from $\bar{\Gamma}$, but it steadily weakens in approaching the band edge. At the same time, the branch γ already at $k_\parallel > 0.04$ Å^{-1} is not a surface resonance, as well as the entire branch α. Note that branch α does not have a spin-orbit split counterpart and, somewhat surprisingly, its polarization does not change sign at $\bar{\Gamma}$. Also in Al/W(110) we observe a stand-alone branch α [Fig. 1(e)], and here its spin polarization is clearly antisymmetric, i.e., spin-↓ for $+k_\parallel$ and spin-↑ for $-k_\parallel$. In Al/W(110) branch β is very pronounced as well, and it is polarized oppositely to the branch α. The branch γ is much less intense in Al/W(110) than in the clean W(110), but it is well discernible in the second derivative of the intensity, especially at higher angles; see Fig. 1(e). This strongly suggests that the branches cross an odd number of times a constant-energy line between $\bar{\Gamma}$ and $\bar{S}$ over a finite energy interval between the bottom of α and bottom of β [see Fig. 1(c)], meaning a behavior topologically different from the simple RB model.

To explain this unusual topology of the energy-momentum distribution of the spin-resolved photoemission in terms of the electronic structure of the W(110) surfaces we show in Figs. 3 and 4 our theoretical spin density distribution. The *ab initio* calculations were carried out in a repeated slab
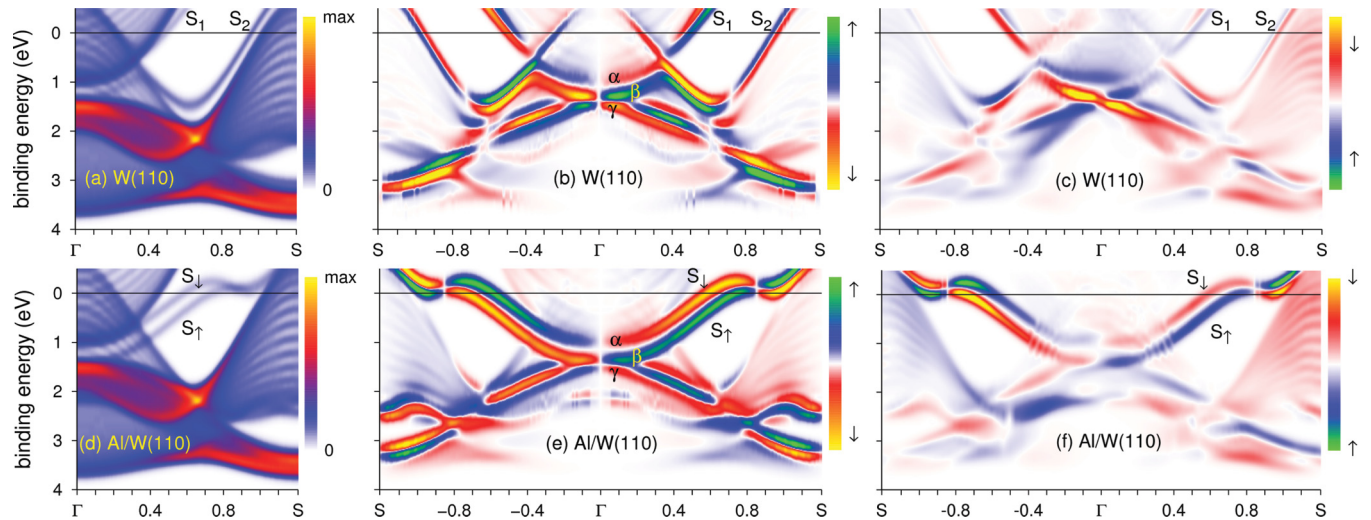
FIG. 3. (Color online) Calculated DOS and SARPES for W(110) (upper row) and Al/W(110) (lower row). $\mathbf{k}_\parallel$ projected DOS $N(E,k_\parallel)$ along $\bar{\Gamma}\bar{S}$: total DOS, (a) and (d); net-spin spectral density $S(E,k_\parallel)$, (b) and (e); net-spin ARPES, (c) and (f).

geometry (29 atomic layers) with the self-consistent (in the local density approximation) full-potential linear augmented plane wave method (LAPW).[22] The relativistic effects were included within the two-component approximation.[23] The total $\mathbf{k}_\parallel$ projected DOS is shown in Figs. 3(a) and 3(d) for W(110) and Al/W(110), respectively. It is defined as a sum over all (discrete) states λ with energy E and Bloch vector $\mathbf{k}_\parallel$: $N(E,\mathbf{k}_\parallel) = \sum_\lambda \delta(E_{\lambda\mathbf{k}_\parallel} - E)$, with the δ function being replaced by a Gaussian of 0.2 eV full width at half maximum. The local depth-resolved $\mathbf{k}_\parallel$ projected DOS is a sum of the densities of spin σ [integrated over a surface parallel plane $z = $ const, with $\mathbf{r} = (\mathbf{r}_\parallel, z)$]: $\rho^\sigma_{\mathbf{k}_\parallel}(z,E) = \int d\mathbf{r}_\parallel \sum_\lambda |\psi^\sigma_{\lambda\mathbf{k}_\parallel}(\mathbf{r})|^2 \delta(E_{\lambda\mathbf{k}_\parallel} - E)$. The net-spin spectral density $S(E,\mathbf{k}_\parallel)$ [Figs. 3(b) and 3(e)] is an integral of the net-spin density $p_{\mathbf{k}_\parallel} = \rho^\uparrow_{\mathbf{k}_\parallel} - \rho^\downarrow_{\mathbf{k}_\parallel}$ over the z interval from the middle of the slab to the middle of the vacuum region. The real-space origin of $S(E,\mathbf{k}_\parallel)$ is revealed

by the partial layer-resolved DOS functions ΔS [Figs. 4(a) and 4(b) for W(110) and Figs. 4(e) and 4(f) for Al/W(110)], where the integration in both cases is over the half space to the right from the topmost W layer, i.e., only vacuum for W(110) and Al layer and vacuum for Al/W(110). The energy-depth charge and spin density distribution is shown for $k_\parallel = 0.1 \text{ Å}^{-1}$ in Figs. 4(c) and 4(d) for W(110) and in Figs. 4(g) and 4(h) for Al/W(110), which demonstrates that the outermost atomic layers are polarized, and in the depth of the crystal there remain weak oscillations of $p_{\mathbf{k}_\parallel}(z)$ with the lattice periodicity.[17]

Clean W(110) hosts two surface states S_1 and S_2, which are both spin split. The spin DOS structure has a clear correspondence to the ARPES intensity dispersion branches indicated in Fig. 1(d): As revealed by Fig. 3(b), the states $S^\downarrow_2$ and $S^\uparrow_2$ connect at $k_\parallel = +0.3 \text{ Å}^{-1}$ to the branches α and β, respectively. Branch β has a higher spin density and extends
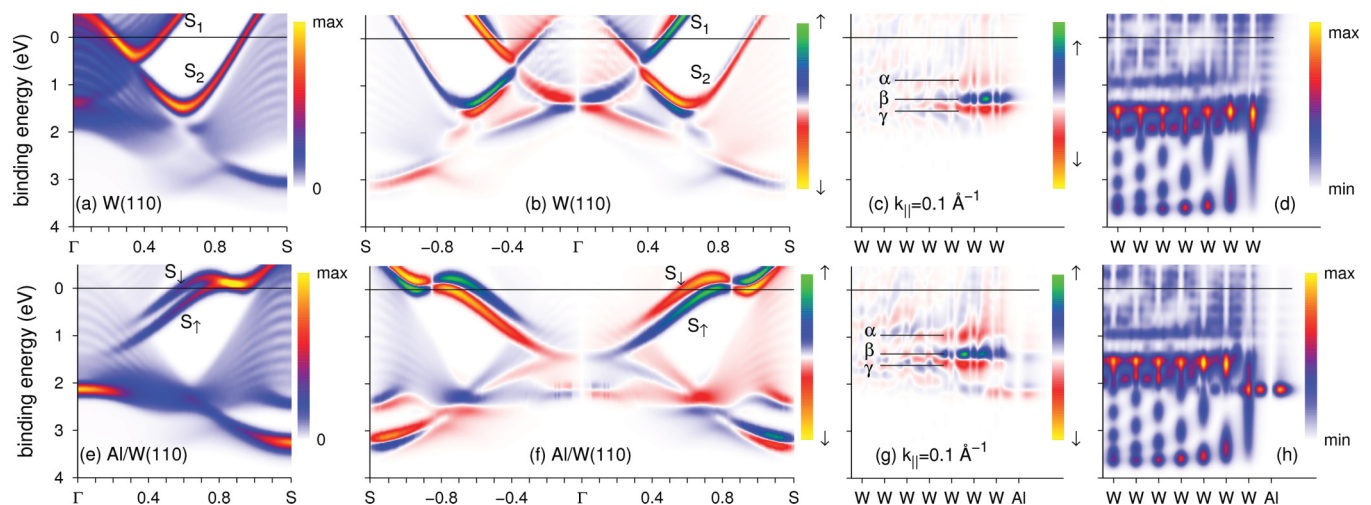

FIG. 4. (Color online) Spatial distribution of the total and net-spin spectral density for W(110) (upper row) and Al/W(110) (lower row). Partial layer resolved DOS, (a) and (e), and net-spin DOS ΔS, (b) and (f), see text. $k_\parallel$ projected local depth-resolved net-spin DOS $p(z,E)$, (c) and (g), and total DOS $\rho(z,E)$, (d) and (h) for $k_\parallel = 0.1 \text{ Å}^{-1}$. One half of the slab is shown, vacuum is to the right. Ticks in the horizontal axis indicate atomic layers. In graph (h) the QWS1 state localized in the Al layer is seen at $E - E_F = -2.1$ eV.
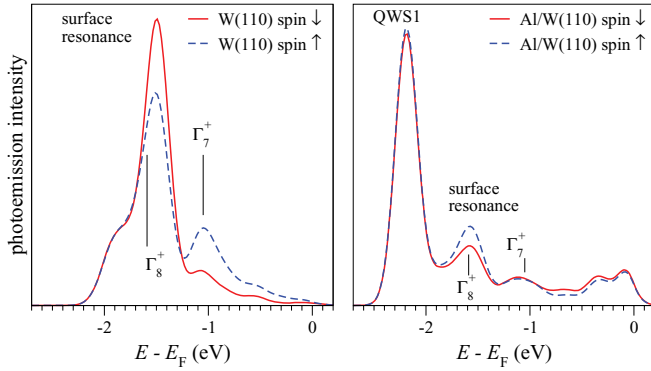
FIG. 5. (Color online) Calculated spin-resolved normal emission EDCs for clean W(110) and for Al/W(110). Photocurrent of spin-↑ is shown by blue dashed lines and spin-↓ by red full lines. Intensity axis is arbitrarily scaled.

further into vacuum than α, as illustrated by Figs. 4(b), 4(c), and 4(d). Branch γ is the opposite-spin counterpart of β: They intersect at $\bar{\Gamma}$ with linear dispersion. The same observation was recently made by Miyamoto *et al.*,[20] who ascribed the feature to the presence of Dirac-cone-like surface states. The present analysis in Figs. 4(a)–4(d), however, shows that at $k_{\parallel} < 0.3$ Å^{-1} the spin-polarized features are of bulk origin.

Such spin structure is indeed characteristic of topological insulators, and here it is established to exist also at a metal surface. This analogy brings about the question of whether the linear dispersion survives a surface perturbation. The answer is offered by the comparison with Al/W(110): Here inside the 3D continuum the branches α and β are retained, but their polarization strongly changes; especially the net-spin density S of branch α around $\bar{\Gamma}$ is enhanced [Fig. 3(e)]. Interestingly, in contrast to the clean W(110) surface, the branches β and γ do not show a linear dispersion at $\bar{\Gamma}$ but go through a turning point. [The splitting of the net-spin-maxima lines in Fig. 1(c) is due to the distributed character of $S(E,k_{\parallel})$ and does not imply a splitting of electronic states.] At the same time, the surface states change dramatically: Instead of the two weakly split pairs S_1 and S_2 we find two strongly polarized states $S_{\downarrow}$ and $S_{\uparrow}$ that connect to α and β, respectively. Here we encounter the "topological metal" behavior: Over a considerable energy interval only branch β as the continuation of the state $S_{\uparrow}$ is present.

To relate the measured spin polarization of the photocurrent to the spin structure of the occupied states, we applied an *ab initio* one-step theory, as described in Ref. 16. Final states are time-reversed low-energy-electron-diffraction states obtained in the scalar relativistic approximation with the inverse LAPW method as explained in Ref. 24. (Spin-orbit effects are negligible at 62 eV.) The inelastic scattering of photoelectrons is included by adding a spatially constant imaginary part $V_i = 2$ eV to the potential in the crystal half space. Calculated EDCs for normal emission are shown in Fig. 5.

In the calculation in Figs. 3(c) and 3(f) the light incidence is fixed at 55° relative to the surface normal, so the left-right asymmetry of the theoretical energy-momentum distribution of the net-spin photocurrent is solely a final-state effect. The photoemission setup breaks the symmetry of the system, so

the spin polarization of the photocurrent does not follow that of the initial states: The total intensity (spin polarization) is not symmetric (antisymmetric) relative to the $\bar{\Gamma}$ point. This final-state effect is, in particular, seen for the $\theta = 0$ spectrum in Fig. 2(a) and the calculated $k_{\parallel} = 0$ spectrum in Figs. 3(c) and 5, which both show the α peak spin-↑ polarized and the β peak spin-↓ polarized, whereas the net-spin density in Fig. 3(b) vanishes by symmetry. Furthermore, both the measured and calculated photocurrent is much more strongly spin-↓ polarized at $-k_{\parallel}$ than spin-↑ polarized at $+k_{\parallel}$. This explains also the spin-↑ polarization of the branch α both for $-k_{\parallel}$ and for $+k_{\parallel}$, which is stronger at $-k_{\parallel}$ in agreement with the experiment.

Finally, we point out an interesting behavior of the $S_{\downarrow}$ and $S_{\uparrow}$ states on Al/W(110) at and above the Fermi level, which is beyond the measured range [Fig. 3(e)]. In approaching the outer border of the gap they both go through an inflection point (falling for $S_{\downarrow}$ and rising for $S_{\uparrow}$ at positive $k_{\parallel}$) and intersect. This means that by tuning the energy of the crossing point relative to E_F (e.g., by surface alloying) one can control the scattering properties of the surface states, because the Bloch vectors and the number of incident and reflected waves rapidly change with energy. Such unusual dispersion close to the Fermi level is interesting for spintronics as it opens a way to manipulate surface spin currents across a 1D boundary.[25]

IV. CONCLUSIONS

To summarize, we have observed how the spin polarization of the surface states on W(110) and Al/W(110) extends into the bulk continuum to connect to spectral spin density branches in the 3D band and form continuous dispersion lines over large $k_{\parallel}$ intervals. This allows us to characterize the spin structure of metal surfaces in terms of the topology of these lines. The analysis of the spin density branches provides important information about the origin and character of surface states. Both in W(110) and in Al/W(110), we have found a topology that strikingly differs both from the case of RB split surface states and from the Dirac cone in topological insulators: The polarization of a single stand-alone branch α changes sign at $\bar{\Gamma}$. At the same time, in W(110) we observe branches with a linear dispersion at $\bar{\Gamma}$ (β and γ), which becomes parabolic upon the deposition of the Al monolayer, as a consequence of their three-dimensional origin. The present theoretical analysis unambiguously establishes that it is the spin structure of the occupied 3D states that underlies the observed spin polarization of the photocurrent but demonstrates that the spin photocurrent does not necessarily reflect the net-spin DOS. Furthermore, we have found a curious behavior of the surface states in Al/W(110): The opposite-spin states intersect just above the Fermi level, which is interesting in the context of spintronics.

---

[1] Y. A. Bychkov and E. I. Rashba, JETP Lett. **39**, 78 (1984); E. I. Rashba, Fiz. Tverd. Tela **2**, 1224 (1960).

[2] M. Z. Hasan and C. L. Kane, Rev. Mod. Phys. **82**, 3045 (2010); X.-L. Qi and S.-C. Zhang, *ibid.* **83**, 1057 (2011).

[3] K. Kuroda, M. Arita, K. Miyamoto, M. Ye, J. Jiang, A. Kimura, E. E. Krasovskii, E. V. Chulkov, H. Iwasawa, T. Okuda, K. Shimada, Y. Ueda, H. Namatame, and M. Taniguchi, Phys. Rev. Lett. **105**, 076802 (2010).

[4] K. Kuroda, M. Ye, A. Kimura, S. V. Eremeev, E. E. Krasovskii, E. V. Chulkov, Y. Ueda, K. Miyamoto, T. Okuda, K. Shimada, H. Namatame, and M. Taniguchi, Phys. Rev. Lett. **105**, 146801 (2010).

[5] S. LaShell, B. A. McDougall, and E. Jensen, Phys. Rev. Lett. **77**, 3419 (1996); M. Hoesch, M. Muntwiler, V. N. Petrov, M. Hengsberger, L. Patthey, M. Shi, M. Falub, T. Greber, and J. Osterwalder, Phys. Rev. B **69**, 241401 (2004).

[6] J. W. Wells, J. H. Dil, F. Meier, J. Lobo-Checa, V. N. Petrov, J. Osterwalder, M. M. Ugeda, I. Fernandez-Torrente, J. I. Pascual, E. D. L. Rienks, M. F. Jensen, and Ph. Hofmann, Phys. Rev. Lett. **102**, 096802 (2009).

[7] D. Hsieh, Y. Xia, L. Wray, D. Qian, A. Pal, J. H. Dil, J. Osterwalder, F. Meier, G. Bihlmayer, C. L. Kane, Y. S. Hor, R. J. Cava, and M. Z. Hasan, Science **323**, 919 (2009).

[8] J. H. Dil, J. Phys.: Condens. Matter **21**, 403001 (2009).

[9] E. Rotenberg, J. W. Chung, and S. D. Kevan, Phys. Rev. Lett. **82**, 4066 (1999).

[10] M. Hochstrasser, J. G. Tobin, E. Rotenberg, and S. D. Kevan, Phys. Rev. Lett. **89**, 216802 (2002).

[11] A. M. Shikin, A. Varykhalov, G. V. Prudnikova, D. Usachev, V. K. Adamchuk, Y. Yamada, J. Riley, and O. Rader, Phys. Rev. Lett. **100**, 057601 (2008).

[12] A. Varykhalov, J. Sanchez-Barriga, A. M. Shikin, W. Gudat, W. Eberhardt, and O. Rader, Phys. Rev. Lett. **101**, 256601 (2008).

[13] A. M. Shikin, A. G. Rybkin, D. E. Marchenko, D. Yu. Usachev, V. K. Adamchuk, A. Yu. Varykhalov, and O. Rader, Phys. Solid State **52**, 1515 (2010).

[14] A. G. Rybkin, A. M. Shikin, V. K. Adamchuk, D. Marchenko, C. Biswas, A. Varykhalov, and O. Rader, Phys. Rev. B **82**, 233403 (2010).

[15] A. G. Rybkin, Ph.D. thesis, St. Petersburg State University, 2010.

[16] A. Kimura, E. E. Krasovskii, R. Nishimura, K. Miyamoto, T. Kadono, K. Kanomaru, E. V. Chulkov, G. Bihlmayer, K. Shimada, H. Namatame, and M. Taniguchi, Phys. Rev. Lett. **105**, 076804 (2010).

[17] E. E. Krasovskii and E. V. Chulkov, Phys. Rev. B **83**, 155401 (2011).

[18] R. H. Gaylord and S. D. Kevan, Phys. Rev. B **36**, 9337 (1987).

[19] E. Rotenberg and S. D. Kevan, Phys. Rev. Lett. **80**, 2905 (1998).

[20] K. Miyamoto, A. Kimura, K. Kuroda, T. Okuda, K. Shimada, H. Namatame, M. Taniguchi, and M. Donath, Phys. Rev. Lett. **108**, 066808 (2012).

[21] D. M. Bylander and L. Kleinman, Phys. Rev. B **29**, 1534 (1984).

[22] E. E. Krasovskii, F. Starrost, and W. Schattke, Phys. Rev. B **59**, 10504 (1999).

[23] D. D. Koelling and B. N. Harmon, J. Phys. C **10**, 3107 (1977).

[24] E. E. Krasovskii and W. Schattke, Phys. Rev. B **59**, 15609 (1999).

[25] F. Meier, V. Petrov, S. Guerrero, C. Mudry, L. Patthey, J. Osterwalder, and J. H. Dil, Phys. Rev. B **79**, 241408 (2009).